Optical and structural studies of some zinc calcium borate glasses for optoelectronic device applications

Hosam M. Gomaa[1], I. S. Yahia[2,3,4], B. M. A. Makram[5,6], Ahmed H. El-Dosokey[7], and Saeid M. Elkatlawy[8,*]

[1] *Independent Researcher, Sakkara Village, Giza, Egypt*

[2] *Research Center for Advanced Materials Science (RCAMS), King Khalid University, P.O. Box 9004, Abha 61413, Saudi Arabia*

[3] *Department of Physics, Faculty of Science, King Khalid University, P.O. Box 9004, Abha, Saudi Arabia*

[4] *Nanoscience Laboratory for Environmental and Bio-Medical Applications (NLEBA), Semiconductor Lab, Department of Physics, Faculty of Education, Ain Shams University, Roxy 11757, Cairo, Egypt*

[5] *Department of Physics, College of Arts and Sciences, Wadi Aldawaser, Prince Sattam Bin Abdulaziz University, AlKharj, Saudi Arabia*

[6] *Physics Department, Faculty of Science, Al-Azhar University, Nasr City 11884, Cairo, Egypt*

[7] *Department of Physics, Faculty of Science, El-Fayoum University, El-Fayoum, Egypt*

[8] *Department of Physics, Faculty of Science, Damanhour University, Damanhour 22111, Egypt*

ABSTRACT

Samples of bismuth borate glasses were prepared by the melt-quenching method, following the molar ratio formula [($58.4-2x$) mol% B_2O_3 + ($18.8 + x$) mol% ZnO + ($18.8 + x$) mol% CaO + 4 mol% Bi_2O_3)], where $x = 0, 2, 4, 6$, and 8 and equal concentrations of zinc oxide and calcium oxide were incorporated into the glass matrix. The structural analysis of the prepared materials was characterized using X-ray diffraction measurements, where each sample showed highly homogenous glassy nature. Deconvolution of X-ray diffraction data was employed to separate unresolved bands, and results manifested the existence of two micro-nucleating agents at 2θ values about 30° and 50°. Optical and optoelectronic properties of the present glasses were assessed using the UV optical absorption. Introducing both zinc and calcium oxides increased the glass transparency for electromagnetic radiation in the UV region. Additionally, values of Fermi energy, Urbach energy, optical conductivity, and the linear refractive index were decreased by the incorporation of both zinc and calcium oxides, while the quality factor was increased. Our results suggest the studied materials for optical filtering, optical switching, and optoelectronic device applications.

Address correspondence to E-mail: saeid.elkatlawy@gmail.com; elkatlawy@sci.dmu.edu.eg

1 Introduction

Oxide glasses (OGs) are characterized basically by their facile and cost-effective mass production, compositional assortment, and their ability to host different elements. Researchers are reporting wide range of applications for oxide glasses, due to the above-mentioned characteristics as well as the facile shaping and processing due to the highly disordered internal structure of OGs and the lack of any crystalline structure [1–5]. Borate-based OGs have been studied in various glass systems for different scientific and technological applications [6–8]. They have strong correlated structure/property relationship and promising linear and nonlinear optical characteristics [9, 10]. They also are characterized by their thermal stability, low melting point, and high transmittance. This makes them unique structures for optoelectronic device manufacturing, solid-state laser media, and luminescent materials [11–14]. Along with the previously mentioned characteristics and fields of applications, researchers are devoted to improving physical properties and increasing the diversity of applications of structures based on borate glasses by adding different dopant elements to the glass matrix [15, 16]. Zinc oxide ZnO is a well-known material for its cost effectiveness, non-toxicity, and environmental acceptability [17, 18]. ZnO can actively play both roles of network former and network modifier in the glass structure and can effectively enhance physical properties of the glass matrix [19, 20]. When playing a modifier role, it breaks the boron-oxygen bond resulting in the formation of non-bridging oxygen defects that leads to changes in the ionic conductivity of the system. However, when acting as a network former, zinc atom links covalently to four oxygen ions, leading to changes in the electronic polarizability and optical basicity of the glass structures [21]. On the other hand, calcium oxide when incorporated in borate-based glass system, it plays the role of a modifier by occupying the network interstitial spaces leading to an increase in the non-bridging oxygen atom, which increases the UV transmission window and overall glass transmittance [22, 23]. Aiming at studying the structure/property relationship of zinc calcium borate-based glasses, lots of studies employing different characterization methods have been carried out. X-ray diffraction (XRD) data deconvolution is a suitable and effective method to separate unresolved bands into several components. This leads to investigating more atomic details and fetch more information that are not accessible directly from experimental data [24, 25]. Optoelectronic device applications depend on the light/matter interaction and the response of electronic processes to light. In this regard, UV–Vis spectral analysis is crucial when studying optoelectronic parameters.

The aim of this article is to study the effect of ZnO and CaO incorporation to bismuth borate glasses on their structural/property relationship. Afterward, optical spectroscopic analysis is employed to study the optical and optoelectronic properties and their relation to the internal structure.

2 Experimental work

In a typical procedure, five glass samples were prepared following the molar ratio formula: $(58.4–2x)$ mol% $B_2O_3 + (18.8 + x)$ mol% $ZnO + (18.8 + x)$ mol% $CaO + 4$ mol% Bi_2O_3) where $x = 0, 2, 4, 6,$ and 8. The raw materials were of high purity, about 99%, were supplied by Semiconductor Lab. Ain Shams University. The prepared batches were placed for 2 h in a muffle oven, adjusted at 850 °C, to obtain homogenous melts, and then quenched on special steel mold, to get solid samples of similar shape and thickness. The prepared solids were checked by XRD technique using X-ray powder diffractometer (Rigaku Miniflex, Japan, CuKα, $\lambda = 1.5406$ Å, radiation from $2\theta = 10°$ to $2\theta = 80°$). Optical measurements were performed using a Jenway 6405 UV–Vis spectrophotometer, in the wavelength range 300–450 nm. For optical measurements, all samples were acknowledged to be of same shape and thickness.

3 Results and discussion

3.1 XRD analysis

The interaction between X-rays and matter produces a sort of interference patterns that give useful information about the material's internal structure. XRD patterns were recorded for the studied samples in the 2θ range from 10° up to 80°, where θ is the angle between the incident X-rays and the internal planes of the sample. These patterns give concise information about structural phase determination and any

sort of strains on the internal structure, in addition to the degree of glass homogeneity. However, the absolute XRD intensity, which is the number of counts per second, can differ because of experimental and instrumental factors. Therefore, it is more appropriate to use relative intensity which is instrument independent. The calculation of relative intensity is obtained by dividing absolute intensity of each peak (hump) by the one for the most intense peak (hump), which is always called the 100% peak, and then convert the result into percentage [26].

Figure 1 depicts the XRD diffractograms for the studied samples. Where the dots represent the experimental XRD pattern for each sample while the solid line refers to the deconvoluted data to facilitate further analysis. By inspecting these graphs, it can be observed that there are no sharp peaks, and only two broad humps are present and located at two different positions, $2\theta \approx 30°$ for high intensity hump and $2\theta \approx 50°$ for low intensity hump. Physically the absence of the sharp peaks means short-range order solids, and the presence of two broad humps refers to two nested networks in the glass system. In other words, each prepared sample showed a good glassy structure formed by two nucleating processes, which is acceptable because both Zn and Bi cations act as micro-nucleating agents, about 30° and 50°, respectively.

Table 1 contains the parameters of peak position $2\theta°$ and the relative area for each hump which is deduced from deconvolution process. Obviously, when the amounts of ZnO and CaO increased, the positions of both humps shifted slightly towards the higher θ values and caused the studied glasses to become more transparent and less dens. This behavior can be interpreted by considering that the atomic radii of both Zn (122 pm) and Ca (176 pm) cations are much larger than that of B^{3+} (85 pm). Also, it can be observed that, as B_2O_3 is replaced by both Zn and Ca cations, the relative area of the left-hand side hump (due to Zn cation) increased, while that of the right-hand side hump (due to Ca cation) decreased, the thing which may be attributed to the relative increases of ZnO and the consequent decreases of B_2O_3.

3.2 UV spectral analysis

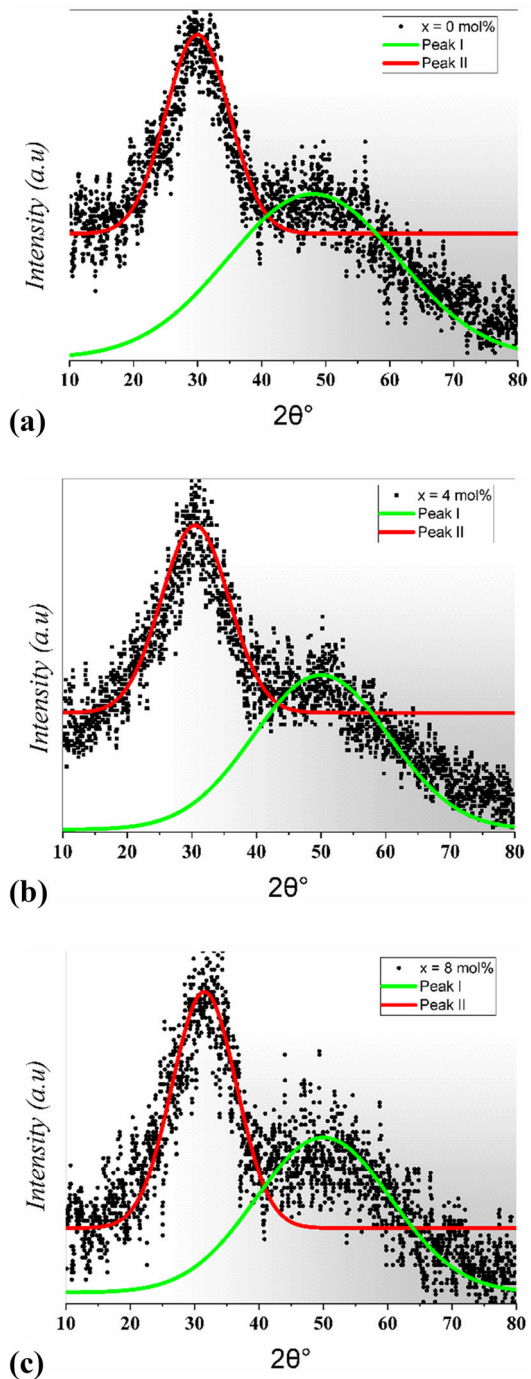The optical parameters were recorded, at room temperature, for the studied samples in the range from

Fig. 1 Experimental and deconvoluted XRD diffractograms for $x = 0$(**a**), 4(**b**), and 8(**c**) samples, other samples show same characteristic

300 to 450 nm. Both the optical absorption A%, Fig. 2, and optical transmittance T%, Fig. 3, were measured for all the studied samples, as a function of wavelength. As illustrated in Figs. 2 and 3, for both A% and T%, when replacing B_2O_3 with equal amounts of

Table 1 XRD-deconvolution obtained parameters

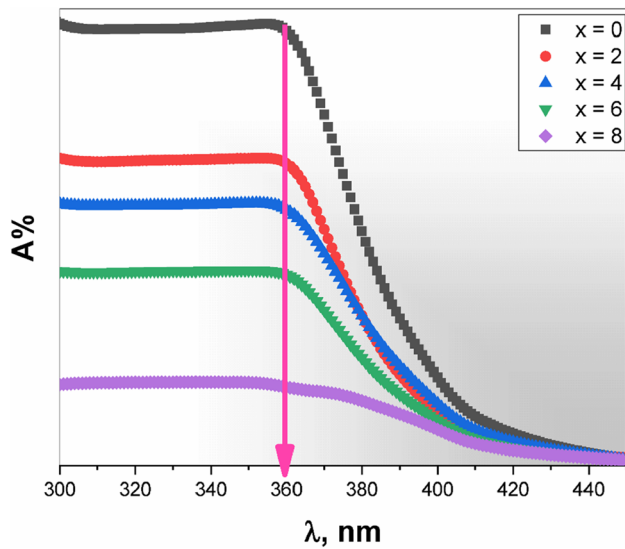| The molar ratio x, mol%	Peak (I)		Peak (II)	
	Peak position $2\theta°$	Relative area under the curve	Peak position $2\theta°$	Relative area under the curve
0	30	84.6	48	15.4
2	30.25	84	48.75	16
4	30.50	83.4	49.5	16.6
6	31	82.2	49.75	17.8
8	31.5	80.6	50	19.5

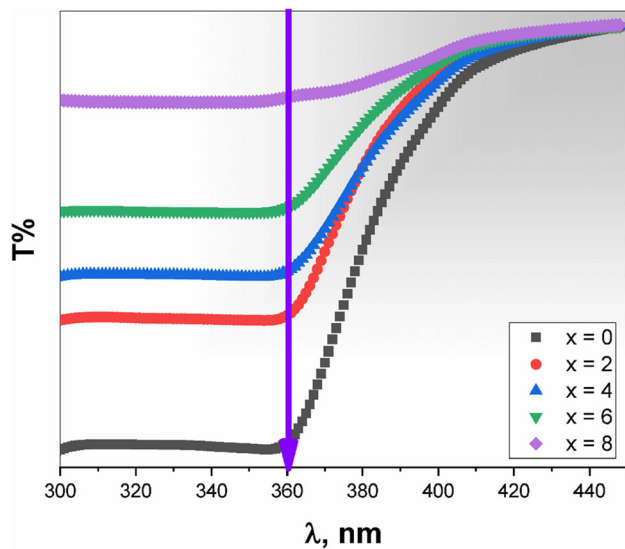**Fig. 2** Absorbance $A\%$ vs. wavelength, for all samples

Fig. 3 Transmittance $T\%$ vs. wavelength, for all samples

ZnO and CaO, these optical parameters showed two opposite behaviors. The increase of Zn^{2+} decreased the optical absorbance while increased the optical transmittance. Such behavior was not expected, where the addition of metal ions should act to increase the probability of the electronic transitions and hence increase the optical absorbance and decrease the optical transmittance. This result can be accepted by considering the structural effects of Ca^{2+}, where it is considered as a glass' network modifier. Because of its large covalent radius (176 pm) which is twice that of boron (85 pm), Ca^{+2} occupies the interstitial vacancies in the glass' network and acts to increase its molar volume, and hence improves the optical transparency. This explanation can be confirmed by referring to the broadness in the width of the XRD humps when the x value increased from 0 to 8. On the other hand, Figs. 2 and 3 show that the behavior of optical absorbance and transmittance was not affected by the incident radiation from 300 to 360 nm. But, when the wavelength increased above 360 nm, the optical absorbance decreased by a constant rate for each sample, x, while the optical transmittance showed an opposite behavior. These observations may suggest the studied glasses for optical filtering and optical switching applications. Based on the measured absorbance and transmittance, the optical reflectance $R\%$, linear refractive index n, and the extinction coefficient k were calculated using the following relations [27–29]:

$$R(\lambda) = 1 - T(\lambda) - A(\lambda), \tag{1}$$

$$n(\lambda) = -\frac{1 + \sqrt{R(\lambda)}}{\sqrt{R(\lambda)} - 1}, \tag{2}$$

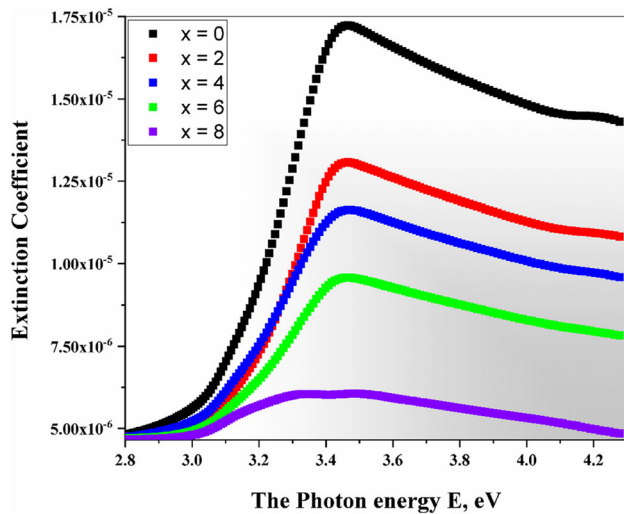$$k(\lambda) = \frac{A(\lambda)\lambda}{4\pi t}. \tag{3}$$

Fig. 4 Extinction Coefficient (*k*) vs. photon energy, for all samples

Extinction coefficient *k* was calculated using Eq. (3) where *t* is the sample thickness, and is presented in Fig. 4 as a function of the energy of incident radiation, at different values of *x*. It is clear that for all values of *x*, the value of *k* increases exponentially by increasing the photon energy up to the maximum value, k_{max}, and then starts to decrease gradually, while the value of k_{max} was found to be decreasing as B_2O_3 was exchanged by equal amounts of ZnO and CaO. Such observation may be apparently noted from the increasing in the glass transparency as a result of an increase in the molar volume, where the covalent radii of both Zn (122 pm) and Ca (176 pm) are much greater than that of boron (85 pm). The extinction coefficient *k* is a useful parameter in determining the value of Fermi energy E_f, based on Fermi–Dirac statistical distribution [30]. Equation (4) is used for the calculation of Fermi energy, where k_B and *T* are the Boltzmann constant and absolute temperature, respectively, while E_{max} is the value of energy at which the extinction coefficient reached to its maximum value k_{max}.

Table 2 Fermi and Urbach energies

x	k_{max}	$E_{max,}$ (eV)	$E_{f,}$ (eV)	E_U (eV)
0	1.7×10^{-5}	3.46	3.17	0.233
2	1.3×10^{-5}	3.55	3.25	0.192
4	1.2×10^{-5}	3.46	3.16	0.185
6	9.5×10^{-6}	3.46	3.15	0.175
8	6.1×10^{-6}	3.42	3.10	0.167

$$E_f = E_{max} - k_B T \ln \frac{1 - k_{max}}{k_{max}}. \qquad (4)$$

Table 2 contains the obtained values for Fermi energy for all studied samples. As seen from the table, the value of Fermi energy decreased as the molar ratio, *x*, increased. This means that, the position of Fermi level shifted toward the valance band as a result of the reduction in the optical absorption, which is consequently associated by an increase in the optical transmission. Such decrease in E_f values may be attributed to an increase in the donor concentrations and/or a decrease in the acceptor one.

Figure 5 illustrates the dependency of the linear refractive index (*n*) on both the sample's structure and the wavelength of the incident photons, this figure indicates that the replacement of B_2O_3 by equal concentrations of ZnO and CaO opens the glass' network structure and hence reduces the light dispersion that occurred in the glasses, leading to an increase in the light velocity through the studied samples. Comparing Fig. 4 by Fig. 5, it can be observed that, the dispersion of the refractive index, *n*, starts when the extinction coefficient *k* reaches its maximum value, therefore, it can be stated that the studied samples may act as an optical filter for all optical energies beyond E_{max} which correspond with k_{max}. Both *n* and *k* values were used to obtain the quality factor Q.F of the studied samples, based on Eq. (5) [31, 32]. As the Q.F does not depend on the shape of the samples, therefore, it is a good tool to compare between the samples under investigation, where in general, it is inversely proportional to the
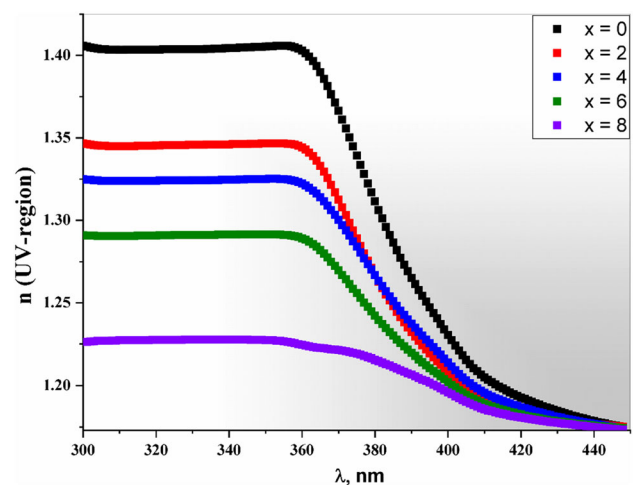

Fig. 5 Linear refractive index vs. wavelength, for all samples

absorption coefficient which represents the intensity of attenuation of light in the glass (i.e., it represents the loss energy). As seen in Fig. 6, the value of Q.F is affected by the exchange of B_2O_3 by equal concentrations of both CaO and ZnO, where the sample with $x = 0.8$ showed the highest Q.F at all photon energies, so it may be suggested for different optical applications.

$$Q.F = \frac{n^2 - k^2}{2nk} \qquad (5)$$

Optical conductivity, which is due to the motion of the charge carriers under the effect of the electric field component of the incident light, is a quantitative property of optical materials. Therefore, values for n and k were used to calculate the optical conductivity σ_{opt} according to Eq. 6, where c is the speed of light in vacuum [29, 33].

$$\sigma_{opt} = \frac{n \, c \, k}{\lambda}. \qquad (6)$$

Figure 7 manifests the energy dependence of the optical conductivities of the studied samples, where in each sample, the optical conductivity increases exponentially with increasing the photon energy up to a certain value at which becomes nearly invariable. Additionally, the optical conductivity decreases with increasing the molar ratio x which may be assigned to the relative decrease in the relative number of the oxygen atoms. Upon this observation, it may be stated that the replacement of B_2O_3 which is a glass network former oxide by an equal amount of both
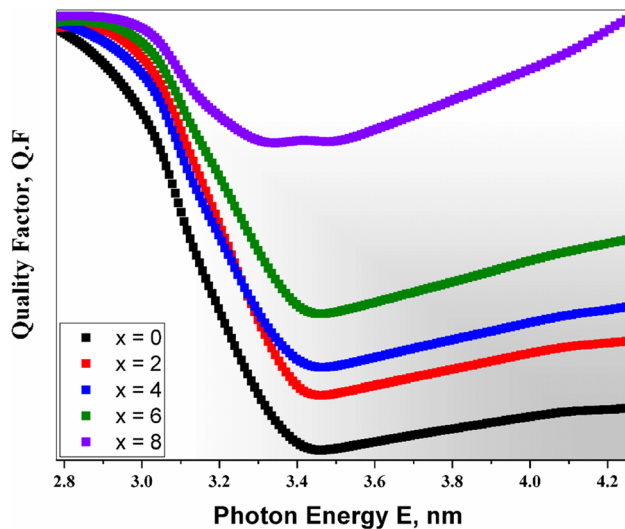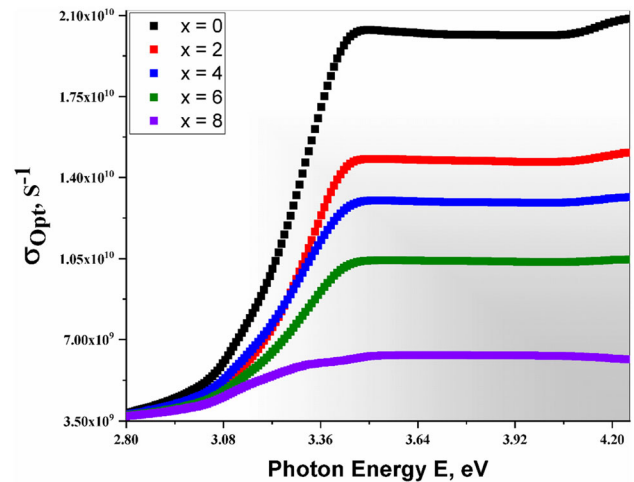

Fig. 7 Energy-dependent optical conductivity for all samples

CaO and ZnO which act as a glass network modifier oxide and a glass network intermediate oxide, respectively, cause a reduction in the optical absorption and further widening in the energy band gap. The higher values of the optical conductivity suggest the studied samples for optoelectronic applications, photo-electric devices, and information processing, in accordance with the literature [34].

3.3 Optical absorption and glass homogeneity

The optical absorption coefficient α is an important tool which is related to the internal structure of the matter. The absorption coefficients of the studied glass samples were calculated using Eqs. (7) and (8) [35–37], where A is the optical absorbance and t is the sample thickness.

$$\alpha = 0.232 \frac{A}{t}, \qquad (7)$$

$$\alpha = \alpha_o e^{\frac{h\nu}{E_U}}, \qquad (8)$$

Urbach absorption mechanism is one of the most used methods to describe the absorption processes that depend on the electronic transitions from an extended state in one band to the localized states in the tail of such band [38]. Such transitions may be originated from the asymmetry of the internal charge distribution that associated with the structural disorders/defects in the studied glasses [38]. Figure 8 depicts Ln (α) versus the incident photon energy ($h\nu$). The slope of the oblique part of the curve was used to estimate the Urbach energy E_U for all samples as
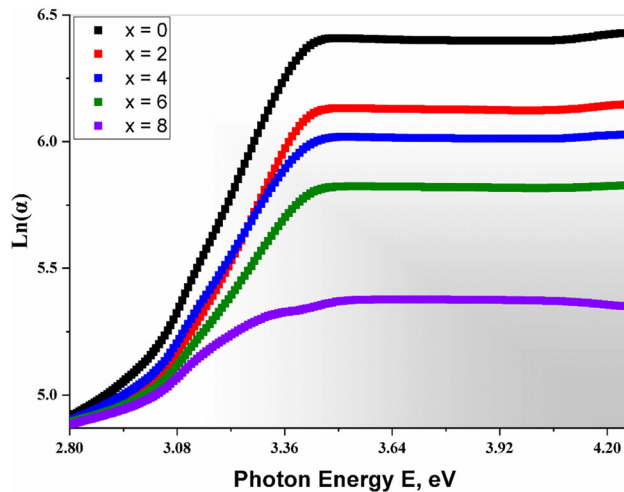

Fig. 6 Q.F for all the studied samples

Fig. 8 The optical absorption coefficient

indicated in Table 2. The decrease in E_U values can be attributed to the increase in the structure randomness which led to more short-range order structure as a result of increasing of both ZnO and CaO contents in the glass samples. The increasing in randomness with increasing x is also confirmed by the XRD chart, where the hump becomes more flatten as x ratio increasing, this is obviously clear in case of sample with $x = 8$ which has the highest homogeneity and the highest short-range order among the studied glass samples.

4 Conclusions

The present work was established to estimate the effect of replacing a glass network former by an equal content of glass network modifier oxide and intermediate oxide, where some bismuth borate glasses doped with equal concentrations of both ZnO and CaO were prepared. XRD structural analysis showed that all samples are of an amorphous nature and have two broad humps. The XRD humps become broader as the contents of both ZnO and CaO increase. The optical parameters showed the strong effect of Ca^{2+} in glass' network modification. The measured optical parameters may suggest the studied glasses to use as optical filters or as devices for optical switching. Also, the optical study showed that the introduction of both ZnO and CaO by an equal amount instead of B_2O_3 increases the optical transparency in the UV spectral region. The calculated values of both Fermi

and Urbach energies suggest the studied glasses for other optoelectronic device applications.

Declarations

Conflict of interest The authors declare that there is no conflict of interest.

References

1. A. Goel, M.J. Pascual, J.M.F. Ferreira, Int. J. Hydrogen Energy **35**, 6911 (2010)
2. A.K. Yadav, P. Singh, RSC Adv. **5**, 67583 (2015)
3. C. Stehle, C. Vira, D. Hogan, S. Feller, M. Affatigato, Phys. Chem. Glas. **39**, 83 (1998)
4. V.V. Dvoyrin, V.M. Mashinsky, L.I. Bulatov, I.A. Bufetov, A.V. Shubin, M.A. Melkumov, E.F. Kustov, E.M. Dianov, A.A. Umnikov, V.F. Khopin, M.V. Yashkov, A.N. Guryanov, Opt. Lett. **31**, 2966 (2006)
5. M. Farouk, A. Samir, F. Metawe, M. Elokr, J. Non Cryst. Solids **371–372**, 14 (2013)
6. G. Padmaja, P. Kistaiah, J. Phys. Chem. A **113**, 2397 (2009)
7. M. Bengisu, J. Mater. Sci. **51**, 2199 (2016)
8. H.M. Gomaa, M.Y. Hassaan, H.A. Saudi, A.S. Morsy, Appl. Phys. A **126**, 391 (2020)
9. D. Ehrt, Glas. Technol. **41**, 182 (2000)
10. Y. Tayal, A.S. Rao, Opt. Mater. (Amst). **107**, 110070 (2020)
11. S. Thomas, S.N. Rasool, M. Rathaiah, V. Venkatramu, C. Joseph, N.V. Unnikrishnan, J. Non Cryst. Solids **376**, 106 (2013)
12. M. Pal, B. Roy, M. Pal, J. Mod. Phys. **02**, 1062 (2011)
13. M. Djamal, L. Yuliantini, R. Hidayat, N. Rauf, M. Horprathum, R. Rajaramakrishna, K. Boonin, P. Yasaka, J. Kaewkhao, V. Venkatramu, S. Kothan, Opt. Mater. (Amst). **107**, 110018 (2020)
14. P.R. Rani, M. Venkateswarlu, S. Mahamuda, K. Swapna, N. Deopa, A.S. Rao, G.V. Prakash, Mater. Res. Bull. **110**, 159 (2019)
15. M.S. Gaafar, N.S.A. El-Aal, O.W. Gerges, G. El-Amir, J. Alloys Compd. **475**, 535 (2009)

16. B. Sumalatha, I. Omkaram, T. Rajavardhana Rao, C. Linga Raju, J. Mol. Struct. **1006**, 96 (2011)

17. B. Sailaja, R. Joyce Stella, G. Thirumala Rao, B. Jaya Raja, V. Pushpa Manjari, R.V.S.S.N. Ravikumar, J. Mol. Struct. **1096**, 129 (2015)

18. G. Rama Sundari, V. Pushpa Manjari, T. Raghavendra Rao, D.V. Satish, C. Rama Krishna, C. Venkata Reddy, R.V.S.S.N. Ravikumar, Opt. Mater. (Amst). **36**, 1329 (2014)

19. S. Cetinkaya Colak, I. Akyuz, F. Atay, J. Non Cryst. Solids **432**, 406 (2016)

20. G.E. El-Falaky, O.W. Guirguis, J. Non. Cryst. Solids **358**, 1746 (2012)

21. M. Abdel-Baki, F. El-Diasty, J. Solid State Chem. **184**, 2762 (2011)

22. S. Sanghi, S. Sindhu, A. Agarwal, V.P. Seth, Radiat. Eff. Defects Solids **159**, 369 (2004)

23. K.S. Manupriya, G.S. Thind, V. Rajendran, K. Singh, A.V. Gayathri Devi, S. Aravindan, Phys. Status Solidi **203**, 2356 (2006)

24. A.M. Abdelghany, Open Spectrosc. J. **6**, 9 (2012)

25. B. Diallo, M. Allix, E. Véron, V. Sarou-Kanian, I. Bardez-Giboire, V. Montouillout, N. Pellerin, J. Non Cryst. Solids **503–504**, 352 (2019)

26. S. A. Speakman, Cent. Mater. Sci. Eng. MIT (2013)

27. Y.B. Saddeek, K. Aly, G. Abbady, N. Afify, K.S. Shaaban, A. Dahshan, J. Non Cryst. Solids **454**, 13 (2016)

28. A.M. El Nahrawy, A.A. Moez, A.M. Saad, Silicon **10**, 2117 (2018)

29. P. Sharma, S.C. Katyal, J. Phys. D. Appl. Phys. **40**, 2115 (2007)

30. M. Khashan, A. El-Naggar, Opt. Commun. **174**, 445 (2000)

31. H.M. Gomaa, J. Non Cryst. Solids **481**, 51 (2018)

32. A.S. Hassanien, J. Alloys Compd. **671**, 566 (2016)

33. S. M. Elkatlawy, A. H. El-Dosokey, and H. M. Gomaa, Boletín La Soc. Española Cerámica y Vidr. (2020)

34. I.S. Yahia, H.Y. Zahran, F.H. Alamri, Synth. Met. **222**, 186 (2016)

35. H.M. Gomaa, I.S. Ali, A.S. Morsy, M.I. Sayyed, Appl. Phys. A **126**, 384 (2020)

36. L. Leontie, M. Caraman, M. Alexe, C. Harnagea, Surf. Sci. **507–510**, 480 (2002)

37. A.S. Hassanien, I.M. El Radaf, A.A. Akl, J. Alloys Compd. **849**, 156718 (2020)

38. R. Naik, J. Pradhan, C. Sripan, R. Ganesan, Phase Trans. **91**, 477 (2018)